

Exceptional conformal anomaly of null polygonal Wilson loops

Harald Dorn ¹

*Institut für Physik der Humboldt-Universität zu Berlin,
Newtonstraße 15, D-12489 Berlin, Germany*

Abstract

We analyse the breaking of conformal invariance for null polygonal Wilson loops in $\mathcal{N} = 4$ SYM beyond that induced by the UV divergences due to the cusps. It only shows up in exceptional configurations, where the polygon intersects the critical light cone of an inversion or a special conformal transformation. In comparison with the related study for the Euclidean version by Drukker and Gross, we find different leading terms both for weak as well as for strong coupling. Hence the conformal anomaly due to intersections of a null polygon with a critical light cone defines a new universal function of the coupling constant.

¹dorn@physik.hu-berlin.de

1 Introduction

Wilson loops for closed smooth contours in $\mathcal{N} = 4$ super Yang-Mills gauge theory are conformally invariant. They have equal values related to the contours before and after a conformal map. This statement needs some specification, because it holds only if both the original as well as the mapped contour are closed in finite domains of space-time. For the Euclidean version the issue has been analysed by Drukker and Gross [1]. They started from the observation that, although an infinite straight line and a circle can be mapped to each other by a suitable conformal transformation, their values are different. They are equal to one (straight line) or equal to a nontrivial function of the coupling constant (circle). This fact has been interpreted as an anomaly with respect to inversions on the unit sphere, emerging as soon as the original closed contour passes the origin of the coordinate system. Under such an inversion the origin is mapped to infinity, and consequently the image contour extends up to infinity and is closed only in the conformal compactification of \mathbb{R}^4 .

In this paper we are interested in the analogous problem in Minkowski space. Now inversions on the unit hyperboloid, as well as special conformal transformations, map a whole critical light cone to infinity. As soon as the original contour intersects such a critical light cone, its image consists out of one or several open pieces forming a closed contour via infinity only. ²

Our focus will be on a certain subset of contours, those for null polygons. They are of particular interest due to their role in the correspondence to scattering amplitudes [2–5].

Now we are faced with another subtlety. Such null polygonal Wilson loops already exhibit breaking of conformal invariance due the UV divergences introduced by their cusps. We have to make a clear separation between this generic conformal anomaly and the exceptional one, showing up only in cases where the null polygon intersects a critical light cone. The former one is present also for infinitesimal conformal transformations and can be controlled by anomalous conformal Ward identities [6]. These Ward identities fix the so-called BDS structure [7], which depends on the *not* conformally invariant Mandelstam variables $X_{jk}^2 = (X_j - X_k)^2$ and allow the freedom of an additional remainder function, depending on the conformally invariant cross-ratios formed out of the X_{jk}^2 . This overall structure is valid for all null polygons closed in a finite domain. As long as we exclude conformal transformations, whose critical light cone cuts the polygon under consideration, we have at hand a covariant form of the renormalised Wilson loops. The change of their values under a conformal transformation originates in the change of the Mandelstam variables only. Therefore, the separation of the exceptional anomaly has to include the definition of a covariant term utilisable in all cases. The anomaly, we are looking for, is then the additional change in the value of the Wilson loop, beyond that originating from the change of the Mandelstam variables in the covariant term.

Obviously, our analysis will require the parallel treatment of Wilson loops for both null polygons closed in a finite domain as well as those for null polygons closed only

²By this we mean closed in the conformal compactification of $\mathbb{R}^{1,3}$.

via infinity. Then we have to keep in mind, that the Mandelstam variables yield an up to isometries unique characterisation only for the ordered sets of null separated points, which serve as vertices. Each pair of consecutive vertices (X_j, X_{j+1}) defines a null geodesic. In forming a null polygon, one then has the option to choose as the related edge either the finite part connecting X_j and X_{j+1} or the complementary part connecting them via infinity. Therefore, to each set of n vertices and their corresponding Mandelstam variables belong 2^n inequivalent null polygons. An analysis of the related classification of conformally equivalent null polygons has been given in [8].

Section 2 will be devoted to the study of the anomaly in lowest order of field theoretical perturbation theory. The behaviour at strong coupling via *AdS/CFT* is studied in section 3. Several technical details are put into two appendices.

2 Anomaly at weak coupling

Analysing the transformation properties of the gluon propagator, Drukker and Gross pinned down the 1-loop anomaly with respect to an inversion on the Euclidean unit sphere to the integral [1]

$$-\frac{1}{16\pi^2} \int dx_1^\mu \int dx_2^\nu \partial_\mu^1 \left(\log \left(\frac{(x_1 - x_2)^2}{|x_1|} \right) \frac{2x_{2\nu}}{x_2^2} \right). \quad (1)$$

As an integral along a closed contour it is zero formally, but due to the singular behaviour at $x_1 = x_2 = 0$ it gives a non-vanishing contribution. Let us consider its Minkowski version for a smooth contour crossing the light cone, centered at the origin, at the point $z \neq 0$, but $z^2 = 0$. For the moment it should have a time-like or space-like tangent vector t at the crossing ($t^2 = \pm 1$). Then with $x_j = z + \sigma_j t + \mathcal{O}(\sigma_j^2)$, ($j = 1, 2$) we get for the factor

$$t^\nu \frac{x_{2\nu}}{x_2^2} = \frac{tz + \dots}{2tz\sigma_2 + \dots} = \frac{1}{2\sigma_2} + \mathcal{O}(1).$$

This is in contrast to the situation for passing the origin (Euclidean case), where $z = 0$ and therefore

$$t^\nu \frac{x_{2\nu}}{x_2^2} = \frac{t^2\sigma_2 + \dots}{t^2\sigma_2^2 + \dots} = \frac{1}{\sigma_2} + \mathcal{O}(1).$$

The relative factor $\frac{1}{2}$ in the two above formulas turns out to be the only difference in the Minkowskian versus Euclidean analysis. Therefore, we can expect that the one-loop anomaly, caused by a single crossing of a critical light cone of a Minkowskian inversion or a special conformal transformation, is just one half of the Euclidean anomaly, as long as the tangent vector of the contour at the crossing point is not light-like.

Since for a closed contour the number of crossings is necessarily even, one could even say that for generic smooth contours the anomaly situation at one-loop level is in some sense the same as in the Euclidean case.

However it is not clear, whether this statement is still true in the limit of a light-like tangent vector at the crossing. If beyond that yet a whole interval on the contour is light-like around the crossing point, the singularity structure of (1) becomes nonlocal. Furthermore, for only piecewise smooth contours one has to disentangle the effect from that of UV divergences due to cusps.

Therefore, we have to perform a careful diagrammatic analysis of Wilson loops for null polygons closed only via infinity. We will do this for the case of four vertices with three of them connected by finite edges. In fig.5 of the next section one can see an illustration of how such a situation arises after a conformal map.

We denote the vertices by X_1 to X_4 , define $p_j := X_{j+1} - X_j$ and the Mandelstam variables as usual by

$$s := (p_1 + p_2)^2, \quad t := (p_2 + p_3)^2. \quad (2)$$

Let us first recall the relevant integrals, see fig.1 for a null tetragon closed within a finite domain, see e.g. [3, 4], $a := \frac{g^2 N}{8\pi^2} \pi^\epsilon \Gamma(1 - \epsilon)$, ϵ parameter of dimensional regularisation, μ RG scale

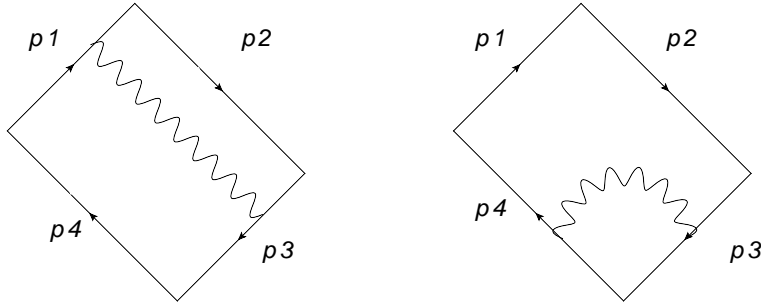


Figure 1: *Two types of contributions for the finitely closed tetragon, on the left J_{13} , on the right J_{34} .*

$$\begin{aligned} J_{13} &= \frac{a}{4} \left(\left(\log \frac{s}{t} \right)^2 + \pi^2 \right), \\ J_{34} &= -\frac{a}{2} \frac{1}{\epsilon^2} \left(\frac{-2p_3 p_4}{\mu^2} \right)^\epsilon. \end{aligned} \quad (3)$$

These formulas are valid for all signs of the Mandelstam variables and yield imaginary parts in case s or t become time-like. Adding the remaining J_{ik} one has altogether

$$\log W(s, t) = a \left(-\frac{1}{\epsilon^2} \left(\left(\frac{-s}{\mu^2} \right)^\epsilon + \left(\frac{-t}{\mu^2} \right)^\epsilon \right) + \frac{1}{2} \left(\log \frac{s}{t} \right)^2 + \frac{\pi^2}{2} \right) + \mathcal{O}(a^2). \quad (4)$$

Now we turn to the Wilson loop for a case with $s < 0$, $t > 0$ and the null polygon going from X_1 to X_2 via infinity, from X_2 to X_3 also via infinity but then with the finite zigzag from X_3 via X_4 back to X_1 . The counterpart to J_{13} is then $\hat{J}_{13} = \hat{J}_{13}^{(1)} + \hat{J}_{13}^{(2)}$, with the two summands related to the two diagrams of fig.2 and given by

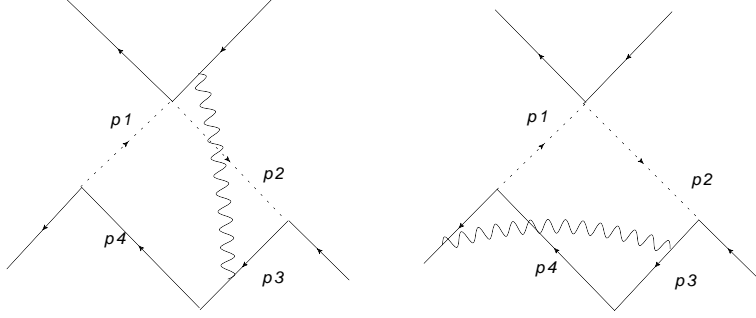


Figure 2: *The two contributions to the counterpart of the first diagram in fig.1, i.e. integration along the p_1 -edge replaced by that along its complement via infinity.*

$$\begin{aligned}\hat{J}_{13}^{(1)} &= \frac{a}{2} (s+t) \int_0^\infty d\sigma_1 \int_0^1 d\sigma_2 (\sigma_1(1-\sigma_2) s - \sigma_2(1+\sigma_1) t - i\varepsilon)^{-1}, \\ \hat{J}_{13}^{(2)} &= \frac{a}{2} (s+t) \int_0^\infty d\sigma_1 \int_0^1 d\sigma_2 (-(\sigma_1+1)(1-\sigma_2) s + \sigma_1\sigma_2 t + i\varepsilon)^{-1}.\end{aligned}\quad (5)$$

Let us look in some detail on the crucial differences in comparison to the calculation of J_{13} for $s < 0$, $t > 0$. There one hits the UV light cone singularity, where the integrand changes its sign. The $i\varepsilon$ -prescription generates an imaginary part and the principal value rule for the real part. Here one has no UV problem, but instead an IR problem. For this the $i\varepsilon$ is irrelevant. The integrand is negative for the first integral and positive for the second one. With a symmetric IR cutoff for the σ_1 -integration we get a finite pure real result (for more details see appendix A)

$$\hat{J}_{13} = \frac{a}{4} \left(\log \left| \frac{s}{t} \right| \right)^2. \quad (6)$$

Obviously we also have $\hat{J}_{24} = \hat{J}_{13}$.

There are three types of cusp contributions. First of all

$$\hat{J}_{34} = J_{34}. \quad (7)$$

\hat{J}_{14} and \hat{J}_{23} are of the same type. To \hat{J}_{14} the two contributing diagrams are depicted in fig.3.

$$\begin{aligned}\hat{J}_{14} &= \frac{a}{2} \int_0^1 d\sigma_2 \left(\left(\frac{-2p_1 p_4}{\mu^2} \right)^\epsilon \int_1^\infty d\sigma_1 (\sigma_1 \sigma_2 - i\varepsilon)^{\epsilon-1} \right. \\ &\quad \left. - \left(\frac{2p_1 p_4}{\mu^2} \right)^\epsilon \int_0^\infty d\sigma_1 (\sigma_1 \sigma_2 + i\varepsilon)^{\epsilon-1} \right).\end{aligned}\quad (8)$$

The σ_1 -integration of the second term is both UV and IR divergent. It is a no-scale integral, which by the standard rules of dimensional regularisation has to be set to zero. Then the evaluation of the first term (as a continuation from the IR-side of ϵ) gives

$$\hat{J}_{14} = -\frac{a}{2} \frac{1}{\epsilon^2} \left(\frac{-t}{\mu^2} \right)^\epsilon = \hat{J}_{23}. \quad (9)$$

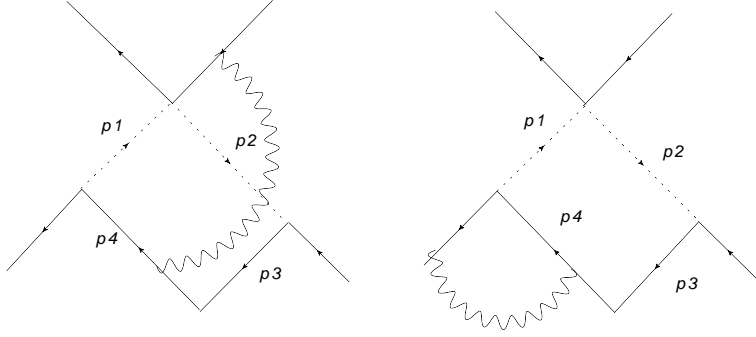


Figure 3: *The two parts of the cusp contribution for the edge p_4 with the complement to p_1 via infinity.*

Note that this equals J_{14} and J_{23} .

The last type of cusp diagrams, which we have to consider, are those for \hat{J}_{12} . They are shown in fig.4. The first three diagrams contain no-scale integrals and can be set

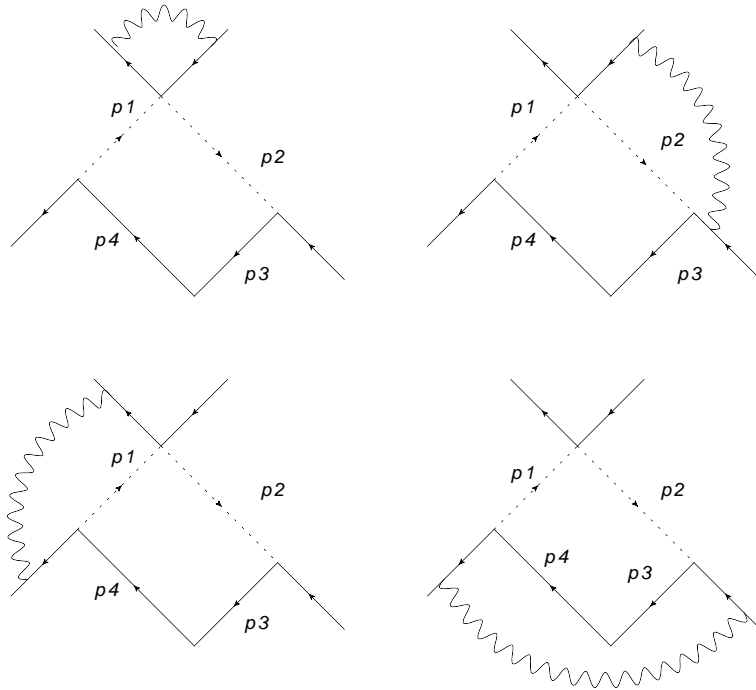


Figure 4: *The four diagrams contributing to \hat{J}_{12} .*

to zero. The last diagram yields

$$\hat{J}_{12} = -\frac{a}{2} \frac{1}{\epsilon^2} \left(\frac{-s}{\mu^2} \right)^\epsilon. \quad (10)$$

Collecting the results from (6),(7),(9) and (10) we get ³

$$\log \hat{W}(s, t) = a \left(-\frac{1}{\epsilon^2} \left(\left(\frac{-s}{\mu^2} \right)^\epsilon + \left(\frac{-t}{\mu^2} \right)^\epsilon \right) + \frac{1}{2} \left(\log \left| \frac{s}{t} \right| \right)^2 \right) + \mathcal{O}(a^2) . \quad (11)$$

Now we have all the ingredients to extract the exceptional anomaly. For this purpose we start with a null tetragon closed in a finite domain with space-like $s, t < 0$. The related Wilson loop is given by eq.(4). If we apply a special conformal transformation, whose critical light cone does not cut the original tetragon, the Mandelstam variables s', t' of the image have the same sign as those of the original, and the image is again finitely closed. The Wilson loop W' for the image is given by the r.h.s. of (4) with s and t replaced by s' and t' , i.e. $\log W' = \log W(s', t')$. Besides this replacement, no further change takes place, i.e. in this case there is no exceptional conformal anomaly.

In contrast, we now apply a special conformal transformation for which one of the vertices, say X_2 is within the critical light cone ⁴ and the others outside. Then W' is a Wilson loop for a null tetragon closed only via infinity. One of the Mandelstam variables has changed its sign ($s' < 0, t' > 0$) and we get from (11)

$$\log W' = \log \hat{W}(s', t') . \quad (12)$$

As long as both Mandelstam variables are space-like $\log \frac{s}{t} = \log \left| \frac{s}{t} \right|$. Then we can declare (4) with the just mentioned absolute value option as *the* covariant term. This gives the exceptional anomaly ('t Hooft coupling λ)

$$\mathcal{C}_2 = -\frac{\pi^2}{2} a + \mathcal{O}(a^2) = -\frac{1}{16} \lambda + \mathcal{O}(\lambda^2) . \quad (13)$$

The index 2 stands for two cuts by the critical light cone. \mathcal{C}_2 is half of the anomaly in the Euclidean case [1] and hence also half of that for generic smooth contours in Minkowski space, as argued at the beginning of this section.

Superficially, there seems to be some arbitrariness in fixing the covariant form. Why, starting from (4) and a configuration with space-like s and t , we insist on using the absolute value option for the argument of the squared log term, but use no absolute values in the divergent pole term? Other choices would generate an imaginary part for the anomaly, which we want to avoid. The absence of an imaginary part for strong coupling will become manifestly in the next section.

3 Anomaly at strong coupling

Within the *AdS/CFT* dictionary, a Wilson loop at strong coupling is given by

$$\log W = -\frac{\sqrt{\lambda}}{2\pi} \mathcal{A} , \quad (14)$$

³Remember that this formula applies to the situation $s < 0, t > 0$ and one vertex connected to the others only via infinity.

⁴In fig.5 it is X_1 . We have a shift in the numbering of vertices between this section and the next one, but hope that this does not confuse the reader.

with \mathcal{A} denoting the area of the minimal surface in AdS_5 approaching the contour of the Wilson loop at the conformal boundary of AdS_5 , [9], see also [1, 2]. Conformal transformations in $\mathbb{R}^{1,3}$ act as isometries in AdS_5 . Therefore, the area of finite surfaces is invariant. The anomaly we are discussing is due to the fact, that we have to handle infinitely extended surfaces for which one can define only regularised areas. Following [2, 10, 12] we use a cut-off at a constant value of the Poincaré coordinate $r = r_c$. The anomaly under a conformal map is then due to the fact, that the image of the boundary of the regularised surface is no longer located at a constant value of r .

To set up some notation, we recall the relation between the embedding coordinates of the AdS_5 hyperboloid in $\mathbb{R}^{2,4}$

$$Y_0^2 + Y_{0'}^2 - Y_1^2 - Y_2^2 - Y_3^2 - Y_4^2 = 1 \quad (15)$$

and Poincaré coordinates:

$$Y^\mu = \frac{x^\mu}{r}, \quad \mu = 0, 1, 2, 3 \quad Y^{0'} + Y^4 = \frac{1}{r}, \quad Y^{0'} - Y^4 = \frac{r^2 - x^\mu x_\mu}{r}. \quad (16)$$

The whole AdS_5 hyperboloid is covered by two Poincaré patches, defined by $r > 0$ and $r < 0$. Its conformal boundary is conformal to two copies of $\mathbb{R}^{1,3}$, corresponding to $r \rightarrow +0$ and $r \rightarrow -0$, respectively.

We consider a minimal surface in AdS_5 with null tetragonal boundary and parameterised in Poincaré coordinates by $(-\infty < \xi, \eta < \infty)$

$$\begin{aligned} r &= \frac{\sqrt{2} a}{\cosh\eta + b \cosh\xi}, & x^0 &= \frac{a \sqrt{1+b^2} \cosh\xi}{\cosh\eta + b \cosh\xi}, \\ x^1 &= \frac{a \sinh\xi}{\cosh\eta + b \cosh\xi}, & x^2 &= \frac{a \sinh\eta}{\cosh\eta + b \cosh\xi}, & x^3 &= 0. \end{aligned} \quad (17)$$

Here $a > 0$, $b \geq 0$ are parameters of isometry transformations in AdS_5 , applied to the initial configuration ($a = 1$, $b = 0$) of ref. [2], given in embedding coordinates as the intersection of $Y_0^2 - Y_{0'}^2 = Y_1^2 - Y_2^2$, $Y_3 = Y_4 = 0$ and the AdS_5 hyperboloid.⁵ This surface is completely located in one Poincaré patch ($r > 0$).

The vertices of the null tetragon approached for $r \rightarrow +0$ are obtained from (17) as follows: X_1 and X_3 in the limits $\xi \rightarrow \pm\infty$, η fix and X_2 and X_4 in the limits $\eta \rightarrow \pm\infty$, ξ fix⁶

$$\begin{aligned} X_1 &= \left(\frac{a \sqrt{1+b^2}}{b}, \frac{a}{b}, 0 \right), & X_2 &= (0, 0, a), \\ X_3 &= \left(\frac{a \sqrt{1+b^2}}{b}, -\frac{a}{b}, 0 \right), & X_4 &= (0, 0, -a). \end{aligned} \quad (18)$$

The related Mandelstam variables are

$$s = (X_1 - X_3)^2 = -4 \frac{a^2}{b^2}, \quad t = (X_2 - X_4)^2 = -4a^2. \quad (19)$$

⁵For details see also the $\theta = \frac{\pi}{4}$ case in ref. [11].

⁶In the notation below we neglect the coordinate x_3 , which is always equal to zero.

Now we want to act with a special conformal transformation in Minkowski space $\mathbb{R}^{1,3}$. Its extension to an isometry of AdS_5 is given by

$$x'^{\mu} = \frac{x^{\mu} + c^{\mu}(x^2 - r^2)}{1 + 2cx + c^2(x^2 - r^2)}, \quad r' = \frac{r}{1 + 2cx + c^2(x^2 - r^2)}. \quad (20)$$

In $\mathbb{R}^{1,3}$ it maps a whole light cone, whose tip is located at $-c^{\mu}/c^2$, to infinity. If this critical light cone cuts an edge of the tetragon, the image of this edge is not completely in a finite domain of Minkowski space, but it is just the piece of the null geodesic connecting the images of the two adjacent vertices via infinity.

Let us choose

$$c = \left(0, \frac{1}{h}, 0\right), \quad (21)$$

then the tip of the critical light cone is located at $x^1 = h$ on the x^1 -axis. Varying h we can study three cases:⁷

Case A: no edge cut,

$$h^2 > \frac{a^2}{b^2} (\sqrt{1+b^2} + 1)^2. \quad (22)$$

Case B: two adjacent edges cut,

$$\frac{a^2}{b^2} (\sqrt{1+b^2} + 1)^2 > h^2 > \frac{a^2}{b^2} (\sqrt{1+b^2} - 1)^2. \quad (23)$$

Case C: all edges cut,

$$\frac{a^2}{b^2} (\sqrt{1+b^2} - 1)^2 > h^2. \quad (24)$$

The situation in *case B* and the image of the tetragon under the special conformal map is illustrated in fig.5.

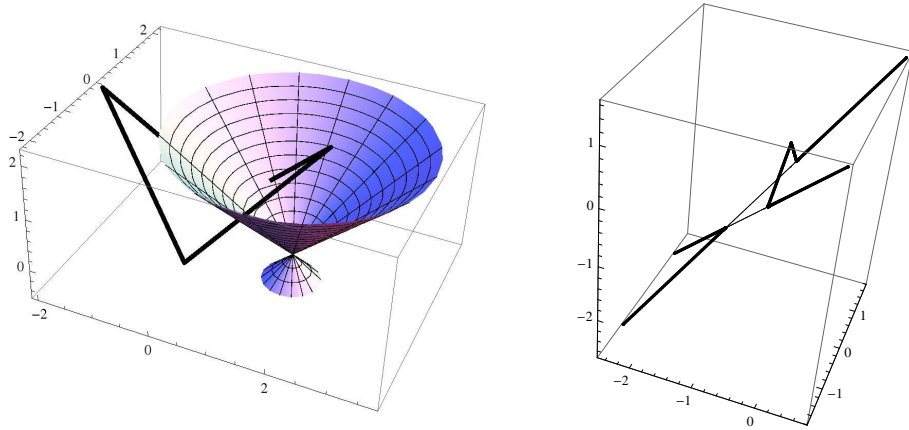


Figure 5: *Tetragon with $a=1$, $b=0.5$ before and after a special conformal transformation. The critical light cone has $h=1.5$.*

⁷Our set-up is symmetric under $h \rightarrow -h$. In the following for convenience we always assume $h > 0$.

The images of the vertices (18) are

$$\begin{aligned} X'_1 &= \frac{h^2}{bh^2 - 2ah - a^2b} \left(a\sqrt{1+b^2}, \frac{ah + a^2b}{h}, 0 \right), & X'_2 &= \frac{h^2}{h^2 + a^2} \left(0, -\frac{a^2}{h}, a \right), \\ X'_3 &= \frac{h^2}{bh^2 + 2ah - a^2b} \left(a\sqrt{1+b^2}, \frac{a^2b - ah}{h}, 0 \right), & X'_4 &= \frac{h^2}{h^2 + a^2} \left(0, -\frac{a^2}{h}, -a \right). \end{aligned} \quad (25)$$

The Mandelstam variables for the image are

$$s' = -4 \frac{a^2}{b^2} \frac{b^2 h^4}{b^2(h^2 - a^2)^2 - 4a^2 h^2}, \quad t' = -4a^2 \frac{h^4}{(h^2 + a^2)^2}. \quad (26)$$

While t' , like the original t , is space-like for all three *cases A,B,C*, we observe

$$s' < 0 \quad \text{in case A and case C}, \quad s' > 0 \quad \text{in case B}. \quad (27)$$

The r -coordinate of the image of the surface (17) under (20),(21) is

$$r' = \frac{\sqrt{2}}{\mathcal{F}(\xi, \eta)}, \quad (28)$$

with

$$\mathcal{F}(\xi, \eta) := \frac{h^2 + a^2}{ah^2} \cosh \eta + b \frac{h^2 - a^2}{ah^2} \cosh \xi - \frac{2}{h} \sinh \xi. \quad (29)$$

By inspection, in *case A* we find r' to be positive in the whole (ξ, η) -plane. For *cases B* and *C* it takes both signs. Furthermore, it goes to $\pm\infty$ along one and two lines in *case B* and *case C*, respectively. Contour lines for three explicit examples are shown in fig.6.

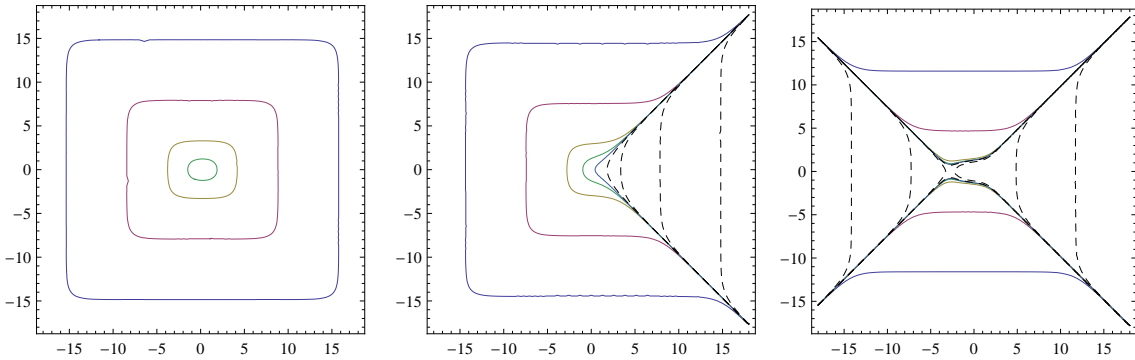


Figure 6: *Contour lines of r' in the (ξ, η) -plane for $a = 1$, $b = 0.5$ and $h = 20$ (case A), $h = 1.5$ (case B) and $h = 0.2$ (case C). Solid lines are for positive r' , dashed lines for negative r' . The chosen values for $|r'|$ are: 10^{-6} , 10^{-3} , 0.1 , 0.6 and in cases B and C also ∞ .*

This pattern reflects the fact that in *case A* the whole image of the original surface is still in the same Poincaré patch, while in *cases B* and *C* it has parts in both patches. At the lines $r' \rightarrow \pm\infty$ it just changes the patch. Of course the mapped surface, as

an embedding in AdS_5 , is smoothly on this lines, since it is obtained by an isometry transformation of the original one. In *cases B and C* its boundary is still a closed null tetragon in the union of the two conformal $\mathbb{R}^{1,3}$ copies constituting the boundary of AdS_5 . The identification of antipodes $Y \sim -Y$ on the hyperboloid (15) induces the standard conformal compactification of $\mathbb{R}^{1,3}$, then the boundary tetragon closes only via infinity.

To define the regularised area of the mapped surface \mathcal{A}_{r_c} , we cut off its parts $0 < r' < r_c$ in the original patch and $-r_c < r' < 0$ in the other one. The induced metric on the space-like minimal surface (17) is

$$ds^2 = -\frac{1}{2} (d\xi^2 + d\eta^2). \quad (30)$$

Using ξ and η also as coordinates on the image of this surface under the AdS_5 isometry (20),(21) we get

$$\mathcal{A}_{r_c} = \frac{1}{2} \int_{\mathcal{B}_{r_c}} d\xi d\eta, \quad \mathcal{B}_{r_c} = \left\{ (\xi, \eta) \mid |\mathcal{F}(\xi, \eta)| < \frac{\sqrt{2}}{r_c} \right\}. \quad (31)$$

Note that this formula holds in all three *cases A, B, C*. With the abbreviations

$$\alpha := b \frac{h^2 - a^2}{2ah}, \quad \beta := \frac{h^2 + a^2}{2ah}, \quad \delta := r_c \frac{\sqrt{2}}{h}, \quad (32)$$

and the change of coordinates $x = \frac{r_c \sqrt{2}}{h} \sinh \xi$, $y = \frac{r_c \sqrt{2}}{h} \sinh \eta$, we arrive at

$$\mathcal{A}_{r_c} = \frac{1}{2} \int_{\mathcal{B}_{r_c}} \frac{dx dy}{\sqrt{\delta^2 + x^2} \sqrt{\delta^2 + y^2}} + o(1), \quad \mathcal{B}_{r_c} = \left\{ (x, y) \mid |F_{r_c}(x, y)| < 1 \right\}, \quad (33)$$

where

$$F_{r_c}(x, y) := \alpha \sqrt{\delta^2 + x^2} + \beta \sqrt{\delta^2 + y^2} - x. \quad (34)$$

The coefficient β is always positive (see (32) and footnote 7) and equal to

$$\beta = \sqrt{-\frac{h^2}{t'}}. \quad (35)$$

For α one finds from (22)-(24) and (26)

$$\begin{aligned} \underline{\text{Case A}}: \quad \alpha &= \sqrt{1 - \frac{h^2}{s'}} > 1, \\ \underline{\text{Case B}}: \quad -1 < \alpha &= \text{sgn}(h - a) \sqrt{\left|1 - \frac{h^2}{s'}\right|} < 1, \\ \underline{\text{Case C}}: \quad \alpha &= -\sqrt{1 - \frac{h^2}{s'}} < -1. \end{aligned} \quad (36)$$

With this information we can characterise the boundary of the asymptotic integration region $B_0 = \lim_{r_c \rightarrow 0} \mathcal{B}_{r_c}$ via

$$F_0 = \alpha |x| + \beta |y| - x = \pm 1. \quad (37)$$

This region is shown for all three *cases* in fig.7. The marked points in the pictures of fig.7 are defined by

$$X_{\pm} := (x_{\pm}, 0) = \left(\frac{1}{|\alpha \mp 1|}, 0 \right), \quad Y := (0, y_0) = \left(0, \frac{1}{\beta} \right). \quad (38)$$

B_0 contains always the quadrilateral $(X_+, Y, X_-, -Y)$. In *cases B* and *C* there is an

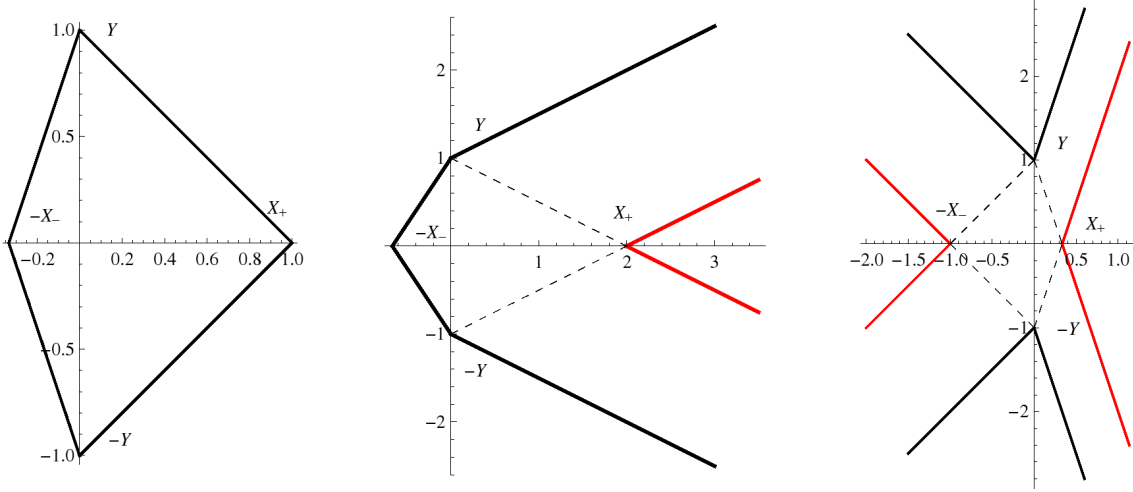


Figure 7: *Examples for the asymptotic integration region B_0 for cases A,B,C with $\beta = 1$ and $\alpha = 2, \frac{1}{2}, -2$, respectively. The black and red lines correspond to Poincaré patches $r > 0$ and $r < 0$, respectively. The dashed lines indicate the subdivision into a quadrilateral and the strips. The axes denote the coordinates x and y .*

additional contribution by two and four semi-infinite strips between parallel straight lines, respectively. These strips are the asymptotic images of the spikes ⁸ in the (ξ, η) -plane (see fig.6) under the map $(\xi, \eta) \rightarrow (x, y)$.

Once again we are not interested in contributions to \mathcal{A}_{r_c} vanishing for $r_c \rightarrow 0$. Therefore, as argued in appendix B, we can in (33) replace the integration region B_{r_c} by B_0 . Then we get

$$\begin{aligned} \underline{\text{Case A:}} \quad \mathcal{A}_{r_c} &= I_{r_c}^{\text{quad}} + o(1), \\ \underline{\text{Case B:}} \quad \mathcal{A}_{r_c} &= I_{r_c}^{\text{quad}} + 2 I^{\text{strip}} + o(1), \\ \underline{\text{Case C:}} \quad \mathcal{A}_{r_c} &= I_{r_c}^{\text{quad}} + 4 I^{\text{strip}} + o(1), \end{aligned} \quad (39)$$

with $I_{r_c}^{\text{quad}}$ and I_{strip} calculated in appendix B as (see (54),(56))

$$I_{r_c}^{\text{quad}} = \frac{1}{2} \log\left(\frac{4x_+x_-}{\delta^2}\right) \log\left(\frac{4y_0^2}{\delta^2}\right) - \frac{\pi^2}{3} + o(1), \quad (40)$$

$$I^{\text{strip}} = \frac{\pi^2}{4} + o(1). \quad (41)$$

⁸Note that these spikes are infinitely long already for $r_c > 0$.

Relating δ to r_c by (32) and expressing the coordinates x_{\pm} and y_0 of the vertices of the quadrilateral via (38),(36),(35) in terms of the Mandelstam variables s', t' , we finally arrive at

$$I_{r_c}^{\text{quad}} = \frac{1}{4} \left(\log \frac{2|s'|}{r_c^2} \right)^2 + \frac{1}{4} \left(\log \frac{2|t'|}{r_c^2} \right)^2 - \frac{1}{4} \left(\log \left| \frac{s'}{t'} \right| \right)^2 - \frac{\pi^2}{3} + o(1). \quad (42)$$

Summarising, the regularised area is given by

$$\mathcal{A}_{r_c} = \frac{1}{4} \left(\log \frac{2|s'|}{r_c^2} \right)^2 + \frac{1}{4} \left(\log \frac{2|t'|}{r_c^2} \right)^2 - \frac{1}{4} \left(\log \left| \frac{s'}{t'} \right| \right)^2 - \frac{\pi^2}{3} + n \cdot \frac{\pi^2}{4} + o(1), \quad (43)$$

with $n = 0, 2, 4$ in *cases A,B,C*, respectively.

In *case A* our result for \mathcal{A}_{r_c} agrees with [10], [11] after $(s', t') \rightarrow (s, t)$.⁹ This confirms covariance under all finite conformal transformations mapping closed null tetragons to closed null tetragons, i.e. only the Mandelstam variables of the original configuration have to be replaced by that of the transformed configuration.

Beyond that we found an anomaly, showing up as soon as the image of the original tetragon is no longer closed in a finite region of Minkowski space. This anomaly for the area \mathcal{A} , relevant for Wilson loops at strong 't Hooft coupling, is given by the pure number $\frac{\pi^2}{4}$ for each crossing of the original null tetragon with the critical light cone of a given finite special conformal transformation. Due to the clear localisation of the anomaly effect in the strips of fig.7 or spikes of fig.6 it seems to be obvious, that this pattern is valid also for higher null polygons. With eq.(14) we get for the exceptional conformal anomaly of the Wilson loop at strong coupling

$$\mathcal{C}_n = -\frac{\pi}{8} n \sqrt{\lambda} + \text{non-leading}. \quad (44)$$

\mathcal{C}_2 has a relative factor $\frac{\pi}{4}$ in comparison with its natural partner in Euclidean space [1, 12].

There is still an interesting side remark. The covariant term in the area, present in all *cases A,B,C* depends only on the absolute values of the Mandelstam variables. Let us for a moment follow a false option: start in the region where both s and t are space-like, replace $(|s|, |t|)$ by $(-s, -t)$ and declare this as the covariant form for the area. Then one would obtain an imaginary part if s and t have different signs.

However, this simply reflects the fact, that there is no minimal surface ending on a null tetragon, closed in a finite region of $\mathbb{R}^{1,3}$, with two space-like and two time-like cusps. Instead, our covariant form plus anomaly contribution yields the area of a minimal surface ending on the null tetragon with the same vertices, but closed via infinity and having space-like cusps only.

⁹And taking into account, that there the Mandelstam variables have been defined with respect to the correspondence with scattering amplitudes, i.e. $(s, t) = 4\pi^2(s, t)|_{\text{there}}$.

4 Conclusions

We have analysed the conformal transformation properties of a Wilson loop in $\mathcal{N} = 4$ SYM for a null tetragon with space-like cusps. As long as the original null tetragon is not cut by the critical light cone of a special conformal transformation, the change of its value is only due to the change of the Mandelstam variables. However if edges are cut, there appears an additional change, which we called exceptional conformal anomaly. At weak coupling we found for two cuts eq.(13) and for strong coupling and two or four cuts eq.(44).

From the details of its genesis in sections 2 and 3 it seems to be quite obviously, that the formulas hold also for higher null polygons. Furthermore, the exceptional anomaly is proportional to the number of cuts. Since this number is necessarily even, the basic entity is

$$\mathcal{C}_2 = \begin{cases} -\frac{1}{16} \lambda + \mathcal{O}(\lambda^2), & \lambda \rightarrow 0, \\ -\frac{\pi}{4} \sqrt{\lambda} + \text{non-leading}, & \lambda \rightarrow \infty. \end{cases} \quad (45)$$

In comparison with the analogous anomaly in the Euclidean case [1, 12] we have a relative factor 1/2 at weak coupling and $\pi/4$ at strong coupling. Therefore, \mathcal{C}_2 defines a new universal function of the coupling λ . Of course it is an interesting open question, whether it appears also in other context.

A nearby issue, which should be answered by a straightforward adaption of our analysis, concerns the even more exceptional situations where the crossing takes places at vertices or where whole edges are located at a critical light cone.

We also argued at the beginning of section 2, that for Wilson loops for generic smooth contours (not null at the crossings with a critical light cone) the anomaly at weak coupling in lowest order is $2\mathcal{C}_2$, in agreement with the Euclidean case. It would be interesting to further clarify, whether this continues in higher orders. Also for strong coupling one can analyse the situation, at least for straight lines and space-like circles with their well-known related minimal surfaces. In the Euclidean case under an inversion on the unit sphere a straight line, not passing the origin, is mapped to a circle. In $\mathbb{R}^{1,3}$ under inversion on the unit hyperboloid e.g. a straight space-like line crossing the light cone and its axis is mapped to a space-like hyperbola. For the area related to a Euclidean circle one has $\mathcal{A} = L(1/r_c - 1/R)$, with $L = 2\pi R$ the circumference of a circle of radius R [12]. In the case of a hyperbola with radius R the circumference is infinite and one is faced with an additional long distance (infrared) problem. Handling it similar to that for the straight line one gets $\mathcal{A} = L_{\text{IR}}(1/r_c - 1/R)$ with a free IR regularisation parameter L_{IR} .

Our discussion necessarily included Wilson loops for null polygons closed only via infinity. Further study should clarify, whether they are connected via some analytic continuation to the finitely closed ones with the same vertices. This touches also the question concerning a possible role in the duality to scattering amplitudes.

Acknowledgement

I would like to thank B. Hoare, G. Jorjadze, M. Staudacher, H.S. Yang and K. Zarembo for useful discussions.

Appendix A

Perhaps the most efficient way to calculate \hat{J}_{13} is to start with

$$J_{13}^{\text{total}} := J_{13} - \hat{J}_{13} = \frac{a}{2}(s+t) \int_{-\infty}^{\infty} d\sigma_1 \int_0^1 d\sigma_2 (\sigma_1(1-\sigma_2)s + \sigma_2(1-\sigma_1)t - i\varepsilon)^{-1}. \quad (46)$$

That \hat{J}_{13} contributes with a relative minus sign is due to its opposite orientation along the contour. The σ_1 -integral is of the type

$$\int_{-\infty}^{\infty} dx \frac{1}{Ax - B - i\varepsilon} = \frac{i\pi}{|A|}. \quad (47)$$

Here the IR problem has been treated with a symmetric cutoff at $x = \pm K$, $K \rightarrow \infty$. Using (47) we get

$$J_{13}^{\text{total}} = \frac{a}{2}(s+t) i\pi \int_0^1 d\sigma_2 \frac{1}{|(1-\sigma_2)s - \sigma_2 t|}. \quad (48)$$

We are interested in the kinematical situation $s < 0$, $t > 0$. Then the σ_2 integrand has no singularity and we get

$$J_{13}^{\text{total}} = \frac{a}{2} i\pi \log\left(\frac{t}{-s}\right) = \frac{a}{2} i\pi \log\left|\frac{t}{s}\right|. \quad (49)$$

Inserting this together with (3) into (46) gives our formula for \hat{J}_{13} used in the main text, (6).

Appendix B

Here we collect the arguments for the replacement of the integration region B_{r_c} in (33) by B_0 , defined in (37), as well as some comments on the calculation of the integrals $I_{r_c}^{\text{quad}}$ and I^{strip} needed in (39).

Let us start with the replacement of B_{r_c} by B_0 . The positive definite integrand for \mathcal{A}_{r_c} in (33) has a uniform r_c -independent bound outside small circles of radius R around the vertices of the quadrilateral $X_+, Y, Y_-, -Y$. Therefore, the contributions to the integrals due to regions of B_{r_c} and B_0 outside these circles differ only by terms vanishing for $r_c \rightarrow 0$. Inside the circles the integrand is bounded by K/r_c with K

some positive constant, depending on the parameters a, b, h and R only. The area between the boundaries of B_{r_c} and B_0 inside these circles vanishes of order r_c^2 . Hence also from inside the circles the contributions to the difference of \mathcal{A}_{r_c} based on B_{r_c} and B_0 vanish in the limit.

Let us sketch the argument for the stated r_c^2 -behaviour of the difference area in the (x, y) -plane, e.g. near the point Y . Here we have to compare the integral $\int(1+x-\alpha|x|)dx$ for B_0 with $(\delta = \sqrt{2}r_c/h)$

$$\int \sqrt{(1+x-\alpha\sqrt{x^2+\delta^2})^2 - \beta^2\delta^2} dx$$

for B_{r_c} . Around $x=0$ the integrand of the last integral can be expanded as

$$(1+x-\alpha\sqrt{x^2+\delta^2}) \cdot (1+O(\delta^2)) .$$

At least now the necessary integrations become trivial.

The quadrilateral integral, used in the main text, is defined by

$$\begin{aligned} I_{r_c}^{\text{quad}} &:= \frac{1}{2} \int_{B_0} \frac{dx dy}{\sqrt{\delta^2+x^2} \sqrt{\delta^2+y^2}} \\ &= \int_{-x_-}^0 \log\left(\frac{y_0(x+x_-) + \sqrt{\delta^2 x_-^2 + y_0^2(x+x_-)^2}}{\delta x_-}\right) \frac{dx}{\sqrt{\delta^2+x^2}} \\ &\quad + \int_0^{x_+} \log\left(\frac{y_0(x_+-x) + \sqrt{\delta^2 x_+^2 + y_0^2(x_+-x)^2}}{\delta x_+}\right) \frac{dx}{\sqrt{\delta^2+x^2}} . \end{aligned} \quad (50)$$

Performing now the trivial part of the x -integration we get

$$\begin{aligned} I_{r_c}^{\text{quad}} &= 2 \log^2 \delta - \log \delta \left(\log(4y_0^2 x_+ x_-) + O(\delta^2) \right) \\ &\quad + \log y_0 \log(4x_+ x_-) + O(\delta^2) + M(x_+, y_0) + M(x_-, y_0) , \end{aligned} \quad (51)$$

with

$$M(m, n) := \int_0^1 \log\left(u + \sqrt{u^2 + \delta^2/n^2}\right) \frac{du}{\sqrt{(1-u)^2 + \delta^2/m^2}} . \quad (52)$$

Replacing the lower integration bound by $\sqrt{\delta}$ we make an error of order $\sqrt{\delta} \log \delta$ vanishing for $\delta \rightarrow 0$. Then we can expand the square root under the logarithm in powers of δ/u and get

$$\begin{aligned} M(m, n) &= \int_0^1 \frac{\log(2u) du}{\sqrt{(1-u)^2 + \delta^2/m^2}} + o(1) \\ &= \log 2 (\log(2m) - \log \delta) - \frac{\pi^2}{6} + o(1) . \end{aligned} \quad (53)$$

Using this in (51) gives

$$I_{r_c}^{\text{quad}} = \frac{1}{2} \log\left(\frac{4x_+ x_-}{\delta^2}\right) \log\left(\frac{4 y_0^2}{\delta^2}\right) - \frac{\pi^2}{3} + o(1) . \quad (54)$$

Finally we calculate ¹⁰

$$\begin{aligned}
I^{\text{strip}} &:= \frac{1}{2} \int_0^{x_+} \frac{dx}{\sqrt{\delta^2 + x^2}} \int_{y_0(1-x/x_+)}^{y_0(1+x/x_+)} \frac{dy}{\sqrt{\delta^2 + y^2}} \\
&+ \frac{1}{2} \int_{x_+}^{\infty} \frac{dx}{\sqrt{\delta^2 + x^2}} \int_{-y_0(1-x/x_+)}^{y_0(1+x/x_+)} \frac{dy}{\sqrt{\delta^2 + y^2}} .
\end{aligned} \tag{55}$$

In the limiting case $\delta = 0$, the only singularity of the integrand is at the point $(x_+, 0)$. It is an integrable one, hence we can perform the limit under the integral. Then with the integrand $\frac{1}{xy}$ the integration becomes trivial

$$I^{\text{strip}} = \frac{\pi^2}{4} + o(1) . \tag{56}$$

References

- [1] N. Drukker, D. J. Gross, *J. Math. Phys.* **42** (2001) 2896 [hep-th/0010274].
- [2] L. F. Alday and J. M. Maldacena, *JHEP* **0706** (2007) 064 [arXiv:0705.0303 [hep-th]].
- [3] G. P. Korchemsky, J. M. Drummond and E. Sokatchev, *Nucl. Phys. B* **795** (2008) 385 [arXiv:0707.0243 [hep-th]].
- [4] A. Brandhuber, P. Heslop and G. Travaglini, *Nucl. Phys. B* **794** (2008) 231 [arXiv:0707.1153 [hep-th]].
- [5] J. M. Drummond, J. Henn, G. P. Korchemsky and E. Sokatchev, *Nucl. Phys. B* **795** (2008) 52 [arXiv:0709.2368 [hep-th]].
- [6] J. M. Drummond, J. Henn, G. P. Korchemsky and E. Sokatchev, *Nucl. Phys. B* **826** (2010) 337 [arXiv:0712.1223 [hep-th]].
- [7] Z. Bern, L. J. Dixon and V. A. Smirnov, *Phys. Rev. D* **72** (2005) 085001 [arXiv:hep-th/0505205].
- [8] H. Dorn, H. Münkler and C. Spielvogel, arXiv:1211.5537 [hep-th]. To appear in “Physics of Particles and Nuclei”.
- [9] J. M. Maldacena, *Phys. Rev. Lett.* **80** (1998) 4859 [hep-th/9803002].

¹⁰We write the explicit defining formula for the right upper strips in fig.7. It will become obviously, that the other strips give the same result.

- [10] L. F. Alday, Fortsch. Phys. **56** (2008) 816 [arXiv:0804.0951 [hep-th]].
- [11] H. Dorn, N. Drukker, G. Jorjadze and C. Kalousios, JHEP **1004** (2010) 004 [arXiv:0912.3829 [hep-th]].
- [12] G. W. Semenoff, K. Zarembo, Nucl. Phys. Proc. Suppl. **108** (2002) 106 [hep-th/0202156].